Electronic Supplementary Material (ESI) for Journal of Materials Chemistry A.
This journal is © The Royal Society of Chemistry 2019

Electronic Supporting Information

Asymmetric superwetting configuration of Janus membranes based on thiol-ene clickable silane nanospheres enabling on-demand and energy-efficient oil-water remediation

Xiangyu Li, Weifeng Zhang, Ruixiang Qu, Yanan Liu, Yen Wei, and Lin Feng*

Department of Chemistry, Tsinghua University, Beijing, 100084, P. R. China

**Corresponding author: fl@mail.tsinghua.edu.cn*

Table of Contents

1. Hydroxyl-rich layer construction on the SSM substrate

Fig. S1a and S1b show that original SSM was woven by cylindrical stainless steel wires with a diameter of nearly 50 μm to form abundant gaps. The surface of original SSM was smooth and clean. Aiming to create Janus layers on the multifarious substrates, the surfaces need to be first hydroxylated for further modification. However, current methods to active surfaces are solely suitable for the minority of subtrates. For instance, Chemical etching approach can deal with common metal or glass substrates but restricted by polymeric surfaces. Despite plasma treatments can active most sustrates, it is limited by multistep procedures and uneconomical instrument processing. Herein, we introduce mussel-inspired catechol chemistry to construct universal hydroxyl-rich layers on various materials, which is implemented via polydopamine (PDA) self-polymerization. After the pretreatment, PDA layer may adhere firmly on the surfaces which can be also visualized through morphological change utilizing field emission scanning electron microscope. As displayed in Fig. S1c and S1d, scattered dots were decorated on the SSM surface, indiating the successful formation of hydroxyl-rich coating that was crucial to subsequent silanization.

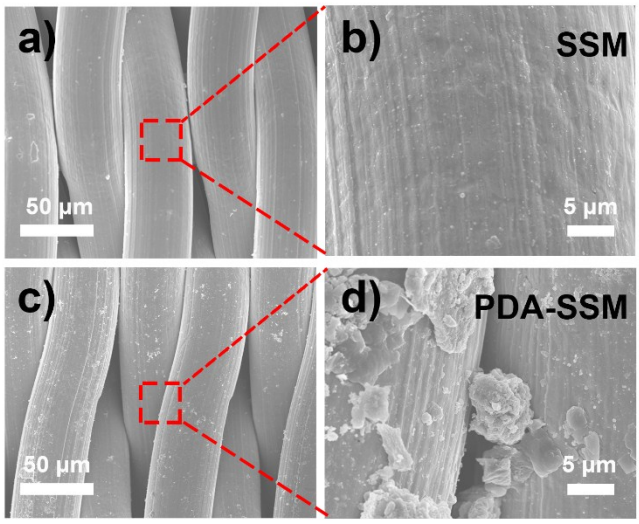

Fig. S1 a) Low and b) high-magnification SEM images of original SSM. c) Low and d) high-magnification SEM images of PDA-SSM.

2. XPS characterization of SSM and PDA-SSM

Fig. S2 shows that the signal of Fe 2p, O 1s and C 1s were detected on the original SSM. In addition, new peak appearing at 401.1 eV (N 1s) was ascribed to PDA self-polymerization on the pretreated SSM.

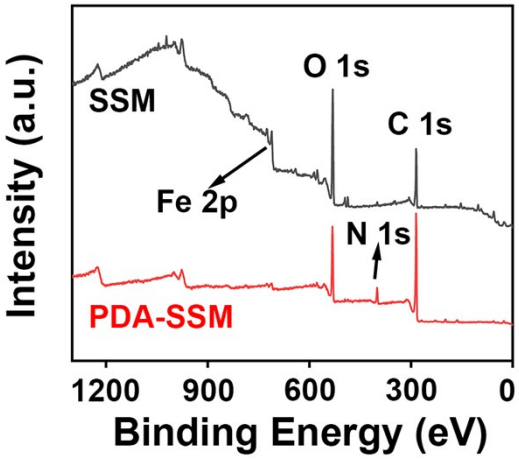

Fig. S2 Wide XPS spectra of original SSM and PDA-SSM.

3. Supplementary explanation of Janus wettability

Paradoxical wetting/antiwetting behavior has been achieved on both sides of the SSM substrate successfully. It is well established that wetting properties is regulated by surface morphology (surface roughness) coupled with chemical composition (surface energy). Owning to the low surface tension of silane, intrinsic hydrophobic nature should be exhibited after TCVS coating. Nevertheless, the final presentation of surface high-hydrophobicity (WCA~145°) was ascribed to the micro/nanostructure formed by varying sizes and irregular stacking of generated silane nanospheres. Cassie-Baxter synergic effect was triggered by the dual-scaled air pockets between the liquid/solid interface that were entrapped into the hierarchical surface morphology as shown in the following equation (S1):

$$\cos\theta^* = f\cos\theta + f - 1 \tag{S1}$$

where θ^* represents the apparent liquid contact angle on the solid surface with rough structure that can store air, θ is the intrinsic liquid contact angle of corresponding smooth solid surface in air and the meaning of f is the effective area fraction of solid phase that is affected by surface roughness. Therefore, enhanced hydrophobicity was presented on the as-prepared mesh due to the increased surface roughness compared with smooth solid surface. In addition, hydrophilic carboxyl group was introduced on the other side of SSM substrate to construct superhydrophilic surface in term of similar wetting model. The excellent underwater oil contact angles (OCA) above 150° was also exhibited regardless of the oil types on the hydrophilic surface, which can be inferred by adhesion work theoretically from the Young-Dupré's equation (S2):

$$W_{ad} = -\Delta G = \gamma_{lv}\left(1 + \cos\theta_{lv}\right) \tag{S2}$$

Where W_{ad} represents the adhesion work, ΔG is the change in surface free energy, γ_{lv} is the surface tension of different liquid and the meaning of θ_{lv} is the corresponding liquid CA on the surface. As a result, the oil phase cannot replace the stored water phase in the micro/nanostructure because the W_{ad} of water was calculated as 144.5 mN m^{-1} that was higher

than those of oils, and the oleophobicity is further amplified by the surface roughness according to Cassie-Baxter equation.

4. Theoretical supplement for on-demand oil/water separaion

Fig. S3a shows the contact angles on three diffent position of the prewetted hydrophobic surface, in which WCA was below 90° without exception. Hence, the high-hydrophobic side is affected to become slightly hydrophilic due to absorbed water phase filled across the whole micro/nanostructure. As exhibited in Fig. S3b and S3c, the Janus-SSM can maintain 200 mm water column but lower than TCVS-SSM (450 mm water column) due to thinner hydrophobic layer.

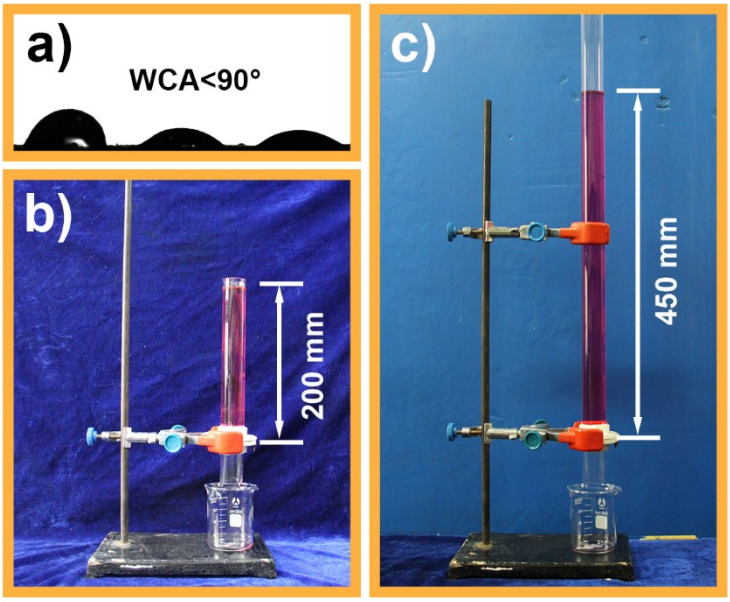

Fig. S3 a) The contact angle of hydrophobic surface was measured at three differnt position after pre-wetting of Janus-SSM. b) The height of water dyed amaranth that the Janus-SSM can endure is 200 mm. c) TCVS-SSM can sustain 450 mm water column.

5. The chemical and mechanical stability of Janus-SSM

1) The chemical stability of the Janus-SSM

In order to comprehensively evaluate the chemical stability of the Janus-SSM, the resistance to strong acid/base solution, high-salt environment and organic solvent were investigated by the SEM images, the water contact angles (WCA) of hydrophobic side and underwater oil contact angles (UOCA) of hydrophilic side after treatment as shown in the Fig. S4. In this part of experiment, the Janus-SSM was immersed in aqueous NaOH solution (0.1 M), aqueous HCl solution (0.1 M), saturated NaCl solution and N,N-dimethylformamide (DMF) for 1 h, respectively. Fig. S4a show that the surface morphologies of the Janus-SSM were nearly unchanged after all four kinds of treatments compared with the original, whether it was unclicked surface or clicked surface. As for the wettability of the two sides, the unclicked surfaces still remained extraordinary high-hydrophobicity (WCA > 140°), and the clicked surfaces possessed underwater high-oleophobicity (UOCA > 140°) despite the slight influence of acid condition (Fig. S4b and S4c). Therefore, the Janus-SSM possessed excellent chemical stability to the extreme environmental conditions, which was ascribed to the chemical inertness of the loaded silanes.

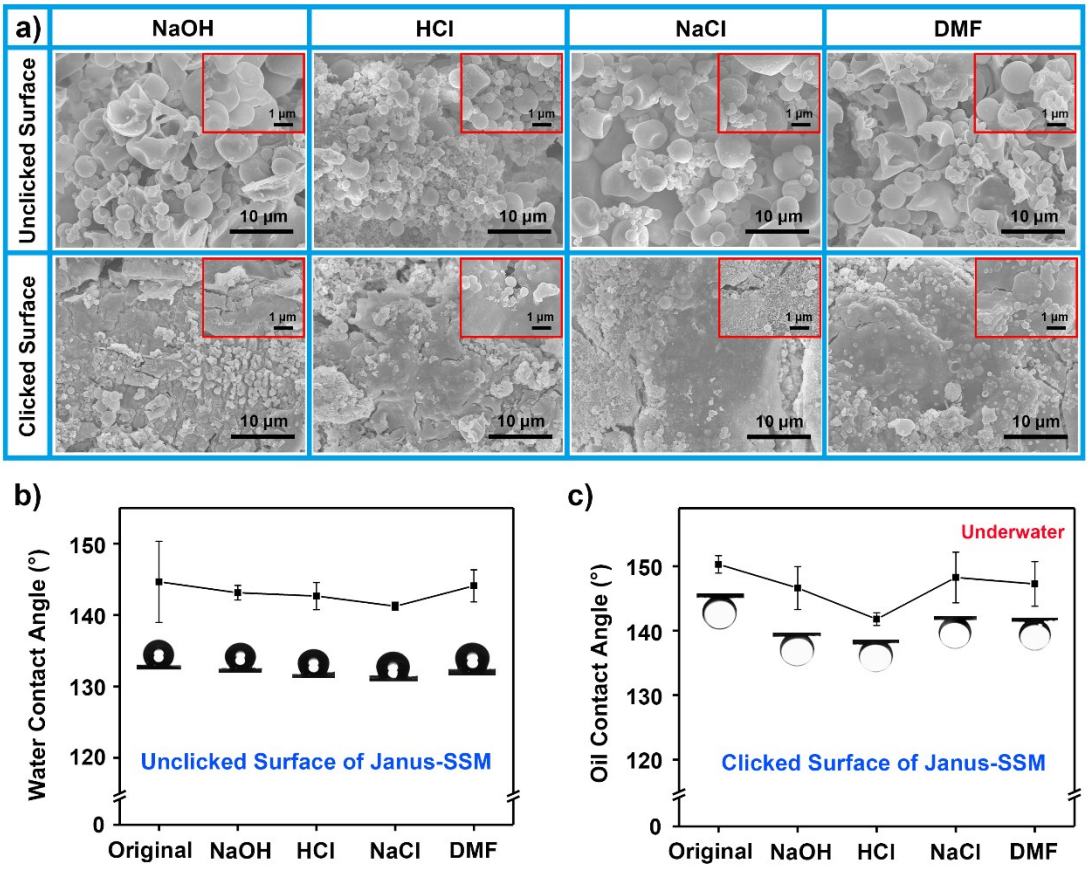

Fig. S4 a) Top SEM images and high-magnification SEM images of the unclicked surfaces and the clicked surfaces of Janus-SSMs after being kept in aqueous NaOH solution (0.1 M), aqueous HCl solution (0.1 M), saturated NaCl solution and dimethylformamide (DMF) for 1 h. b) The WCAs of the unclicked surfaces under after different treatment. c) The UOCAs of the clicked surfaces under corresponding treatment (the used oil was petroleum ether).

2) The mechanical stability of the Janus-SSM

There is no doubt that the mechanical stability is of great significance for the practical applications of Janus-SSM. Herein, the mechanical durability to resist external forces was qualitatively evaluated by the ultrasonic treatment test in ethanol for 1 h. The WCAs of the unclicked surafce and the UOCAs of the clicked surface after each 10 minutes of ultrasonic treatment were recorded as shown in Fig. S5a and S5c. With the increase of unltrasonic time, the WCAs remained greater than 140°, and the rough microscopic morphology of the unclicked surface still retained similar to that before one-hour ultrasonic treatment except for slight

decrease in the amount of silane nanospheres as shown in Fig. S5b. With regard to the clicked surface, the underwater oleophobicity gradually decreased along with the extension of the ultrasonic time. This phenomenon can be attribute to the loss of microscale silane aggregations and reduced roughness in term of the SEM images after ultrasonic treatment (Fig. S5d). Notably, the clicked surface still had its oil repellency even being seriously damaged by one-hour ultrasonic vibration (UOCA > 135°). Baced on the above-mentioned results, the as-prepared Janus-SSM had considerable mechanical stability, which was derived from the great adhesive force to substrate of the covered silanes.

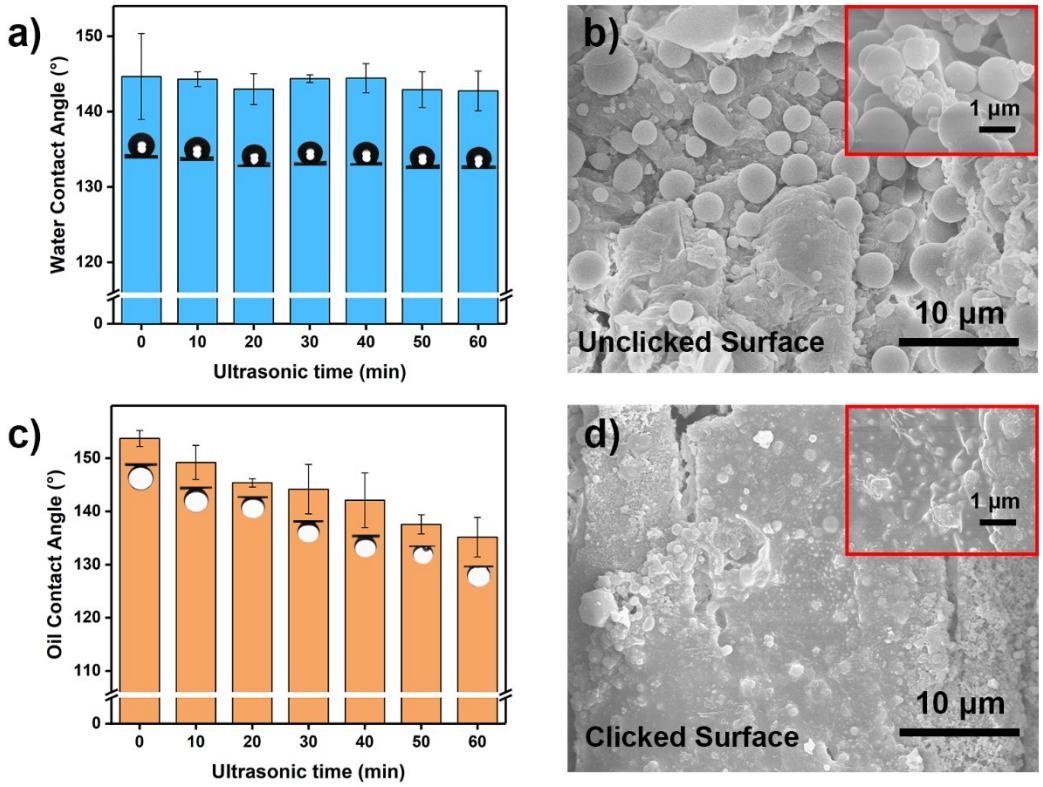

Fig. S5 a) The effect of ultrasonic time on the WCAs of the unclicked surface of the Janus-SSM. b) Top SEM image and high-magnification SEM image of the unclicked surface of the Janus-SSM after ultrasonic treatment in ethanol for 1 h. c) The effect of ultrasonic time on the UOCAs of the clicked surface of the Janus-SSM. d) Top SEM image and high-magnification SEM image of the clicked surface of the Janus-SSM after ultrasonic treatment in ethanol for 1 h.

6. The effect of the water content on the microscopic morphology and the oil/water separation performance

In order to investigate the effect of the water content on the microscopic morphology and the oil/water separation performance, the corresponding water content gradient tests were conducted, in which stainless steel mesh (SSM) substrate was taken as an example for illustration. In this part of the experiment, the original water volume (300 μL) in the toluene (100 mL) was extended by three additional gradients including 200 μL, 400 μL and 500 μL.

It can be observed that different microscopic morphologies were formed on the SSM substrate by regulating the added water volume via field emission scanning electron microscope (Fig. S6a). When the added water volume was 200 μL, only a few silane nanospheres were anchored on the surface, indicating the incomplete hydrolysis and polycondensation of TCVS. Noteworthily, a significant increase of silane nanospheres was exhibited upon increasing the water volume to 300 μL. However, the surface topography did not produce distinct changes except for the continuous increase of silane nanospheres with further increase of the water volume (400 μL and 500 μL). As for the worse solubility of water in toluene, the increase of silane nanospheres can be explained from the perspective of the reaction solvent system. Although the added water would not be completely soluble in toluene, the whole reaction solvent system has formed one type of water-in-toluene emulsion in the process of ultrasound. It is worth noting that TCVS was excessive compared to the added water. When the substrate was placed in such system, TCVS underwent hydrolysis in the water micro drops and further combined with the hydroxyl-rich layer on the substrate. Hence, more water would induce more TCVS hydrolysis to construct more silane nanospheres on the surfaces.

As described above, the microscopic morphology was controlled by the water content, which would affected the surface wettability due to the regulated surface roughness. Fig. S6b shows the water contact angles (WCA) on the surfaces of aforementioned TCVS-SSMs at different water contents. The WCA of the as-prepared mesh at the water volume of 200 μL was

122.7° indicative of the poor hydrophobicity. When the water volume reached 300 μL, the surface hydrophobicity was greatly enhanced which can be seen from the WCA up to 144.7°. In addition, a slight increase of hydrophobicity can be observed with further increasing water volume. It is worth noting that such surface wettability would impact oil/water separation performance of the materials. Herein, each TCVS-SSM was prepared into the corresponding Janus-SSM under the same conditions and chloroform/water mixture (heavy oil/water mixture) was chosen as representative sample to evaluate the separation performance. As expected, the trend of oil/water separation efficiency was similar to that of surface hydrophobicity (Fig. S6c). The separation efficiency of the Janus-SSM at the volume of 200 μL was obviously below the other meshes. Moreover, separation efficiency of the materials basically remained unchanged when the water volume was above 300 μL.

In summary, more silane nanospheres can be decorated on the substrate with the increase of water volume. When added water volume was above 300 μL, the material would possess excellent hydrophobicity and oil/water separation performance. From the perspective of materials consumption, the water volume of 300 μL was enough to deal with oil/water mixtures.

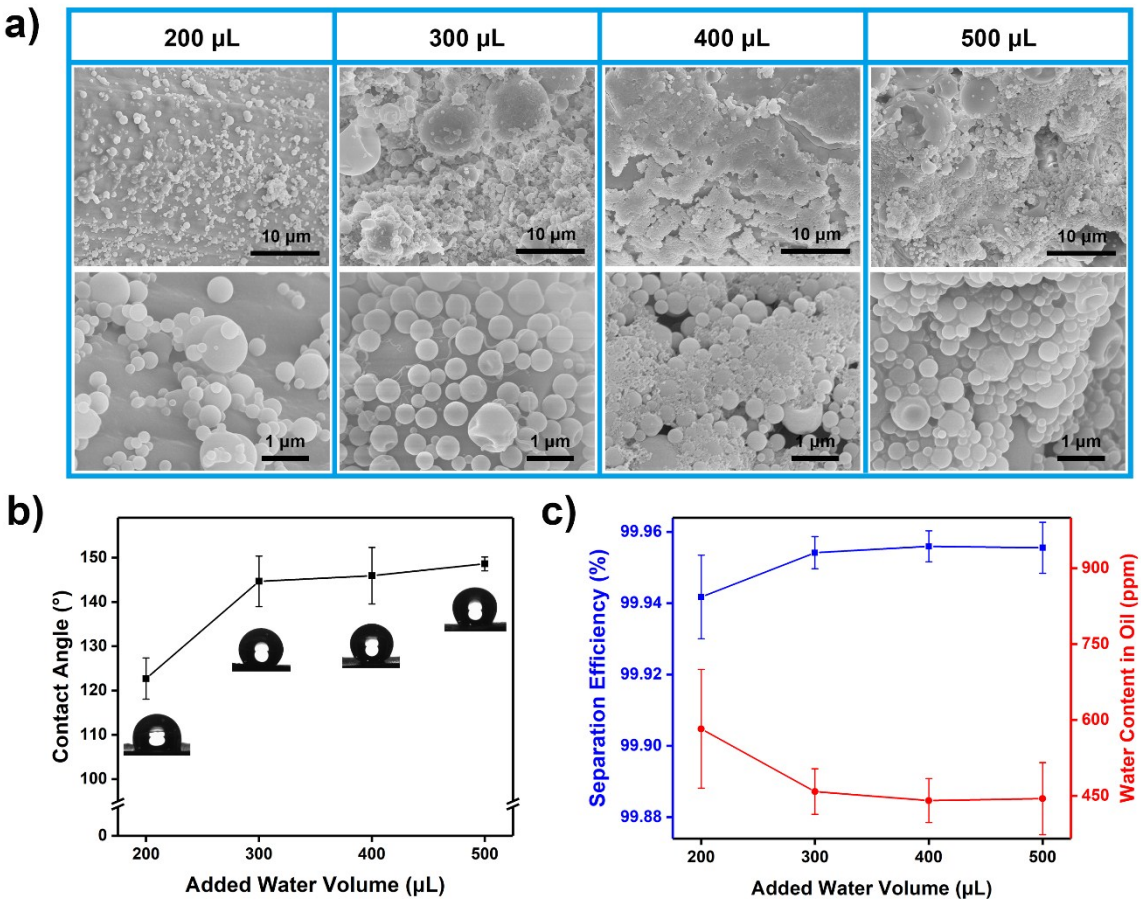

Fig. S6 a) Top SEM images and high-magnification SEM images of TCVS-SSMs at different added water volumes. b) WCA in air of TCVS-SSMs at different added water volumes. c) Separation efficiency and corresponding water content of the filtrates in heavy oil/water mixture separation for Janus-SSMs at different added water volumes.

7. Surface morphology of PVDF, PDA-PVDF and TCVS-PVDF

The high porosity and ultrathin thickness of PVDF membrane are of importance to the liquid permeation flux in terms of the Hagen-Poiseuille equation (S3).

$$J = \frac{\varepsilon \pi {r_{\text{pore}}}^2 \Delta P_{\text{t}}}{8 \mu L} \tag{S3}$$

Where J respresents the liquid permeation flux, ε means the membrane porosity, r_{pore} is the effective radius of the pore, ΔP_{t} is the total pressure, μ is the viscosity of the liquid and L is the thickness of the membrane. As displayed by the SEM images in Fig. S7a and S7b, the pristine PVDF membrane possessed three-dimensional porous structure. After hydroxylation with PDA and silanization with TCVS, silane nanospheres coating was assembled successfully on the surface (Fig. S7c-f).

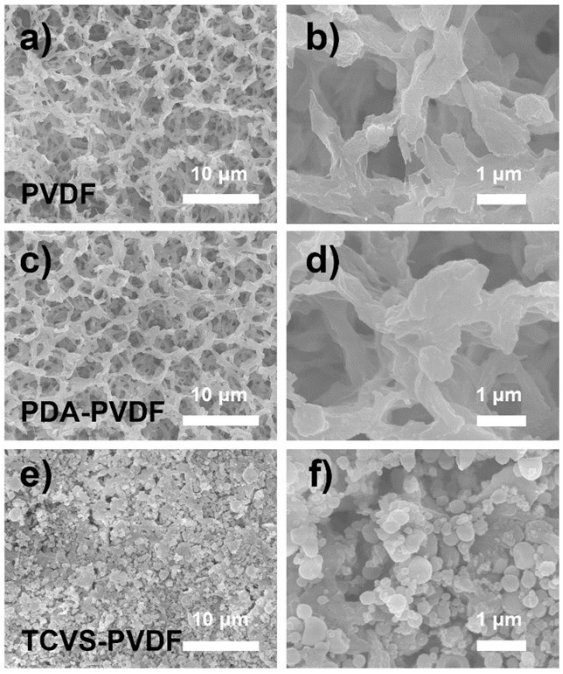

Fig. S7 a) Low and b) high-magnification SEM images of pristine PVDF. c) Low and d) high-magnification SEM images of PDA-PVDF. e) Low and d) high-magnification SEM images of TCVS-PVDF.

8. Chemical composition characterization of the precursors

The formation of silane coating can be confirmed precisely by EDX mapping (Fig. S8), in which 16.8wt% Si element was detected on the TCVS-PVDF membrane surface. Fig. S6a shows the XPS spectra results of these precursors, obviously, the presence of Si 2s and 2p signals on TCVS-PVDF was in agreement with EDX mapping. As exhibited in Fig. 4f and Fig. S9b, the unclicked surface of Janus-PVDF remain C 1s core-level spectrum similar to that before processing, realizing the asymmetric surface configuration on the two sides.

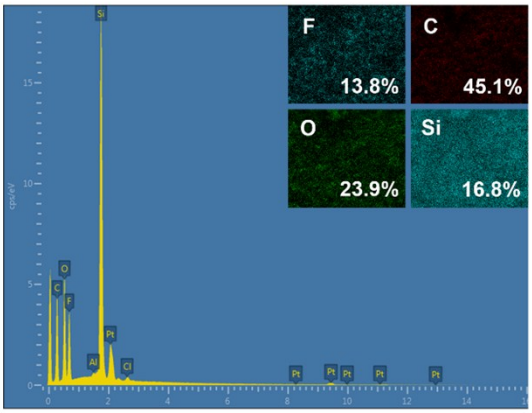

Fig. S8 a) EDX mapping of TCVS-PVDF.

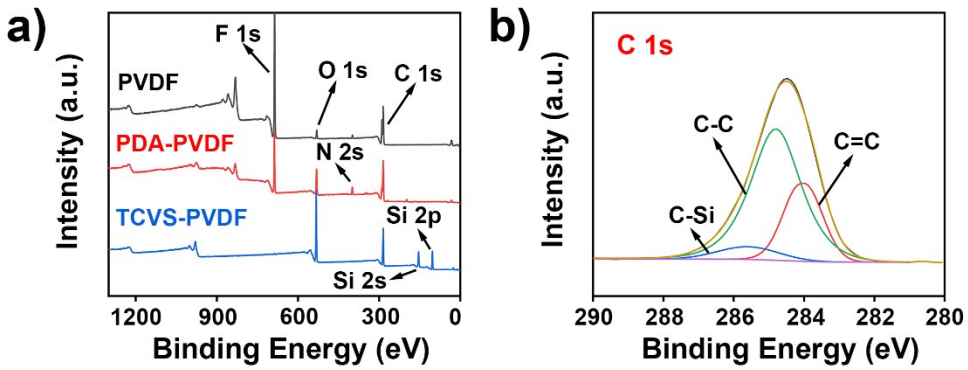

Fig. S9 a) Wide XPS spectra of original PVDF, PDA-PVDF and TCVS-PVDF. b) The high resolution XPS spectra near C 1s region of TCVS-PVDF.

9. The AFM images of TCVS-PVDF before and after UV irradiation

In order to clearly show the difference of the surface before and after UV irradiation, different areas of each surface were measured by atomic force microscope to obtain the average roughness (Rq) of the full view (Fig. S10). Since there was no big difference among these areas, the average Rq could be the representative roughness of the surface. According to the AFM images, the silane nanospheres collapsed or disappeared after UV irradiation, resulting in a great discrepancy of surface roughness (Rq) from 216.26 nm to 330.53 nm. The aforementioned results indicated an obvious occurrence of thiol-ene click reaction.

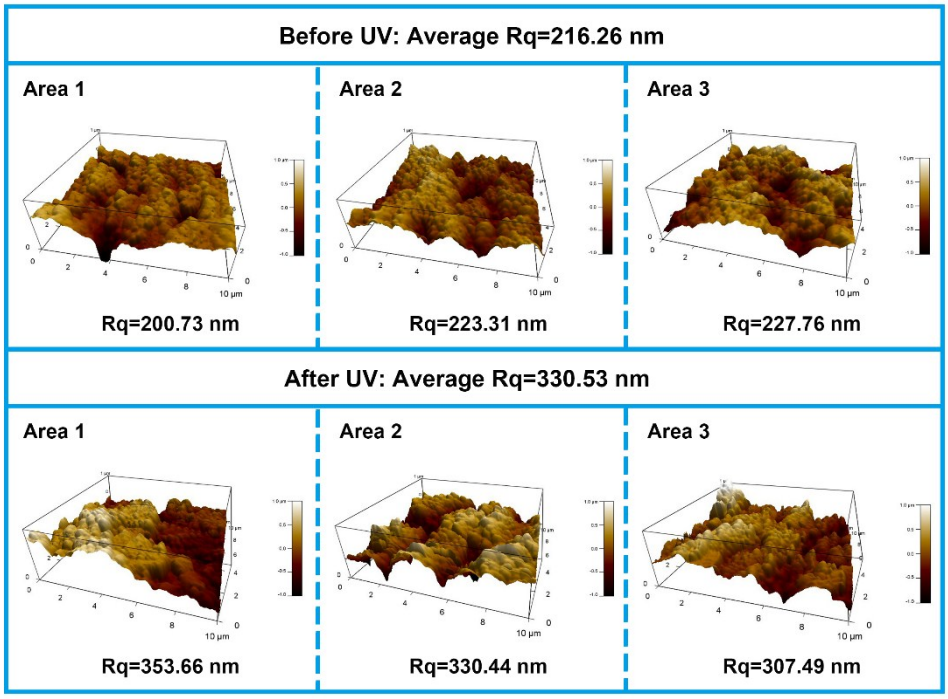

Fig. S10 The AFM images and the corresponding average roughness of the upper surface of TCVS-PVDF before and after UV irradiation, respectively. Several different areas of each membrane were observed and the Rq was taken average.

10. Droplet size and distribution of surfactant-stabilized emulsions

As demonstrated in Fig. S7, numerous droplets with the average size of about 10 μm were dispersed in the oil-in-water and water-in-oil emulsions, meaning the difficulty of separating dispersed phase from the continuous phase.

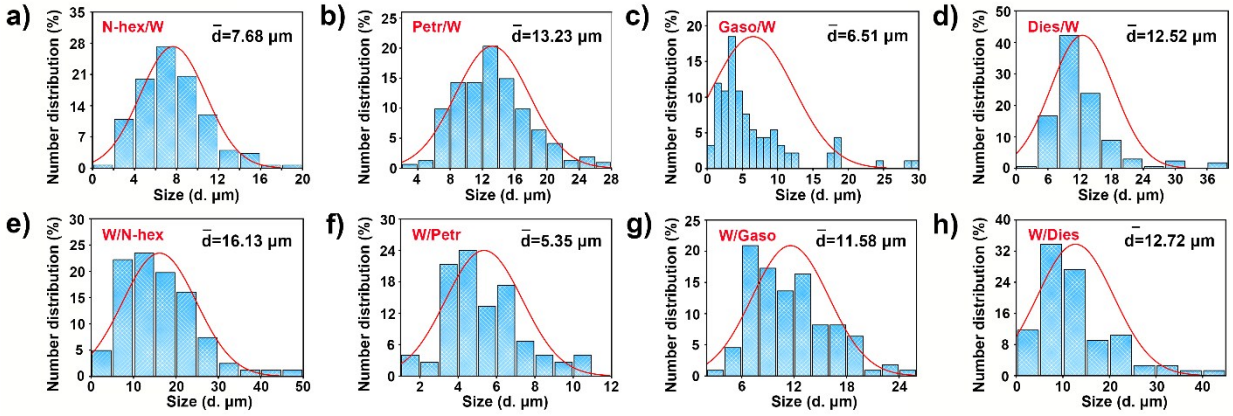

Fig. S11 The average droplet size and distribution of the surfactant-stabilized emulsions including a) n-hexane-in-water, b) petroleum ether-in-water, c) gasoline-in-water, d) diesel-in-water, e)water-in-n-hexane, f) water-in-petroleum ether, g) water-in-gasoline, h) water-in-diesel.

11. The stability of the as-prepared emulsions

In order to evaluate the stability of the as-prepared emulsions, corresponding emulsion stability tests were carried out. It was obvious that all the emulsions were still stable without demulsification for at least 3 days whether oil-in-water type or water-in-oil type, demonstrating the excellent performance of the Janus membrane.

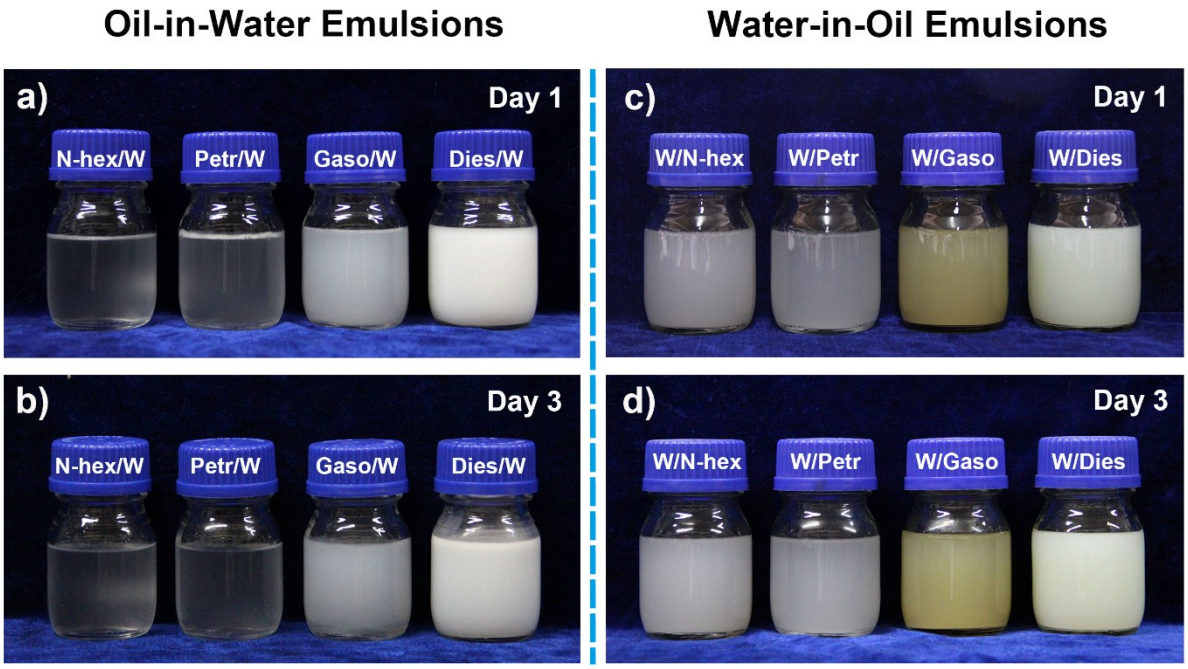

Fig. S12 a) and b) The stability test of the oil-in-water emulsions. c) and d) The stability test of the water-in-oil emulsions.

12. The chemical and mechanical stability of Janus-PVDF

1) The chemical stability of the Janus-PVDF

Likewise, the aforementioned processing conditions were applied to the Janus-PVDF to evaluate the chemical stability of this type of Janus materials. To investigate the surface state of the Janus-PVDF after treatment, morphology observation was performed in the Fig. S11a, which indicated that the surfaces were not been destroyed by the corrosive condition. Moreover, the effects of these rigorous conditions on the wettability of both sides were exhibited in Fig. S11b and S11c, respectively. The results show that the WCAs of the unclicked surface were essentially unchanged and the UOCAs of the clicked surface had a little decrease but were still higher than 145°, demonstrating the outstanding resistance to extreme environment.

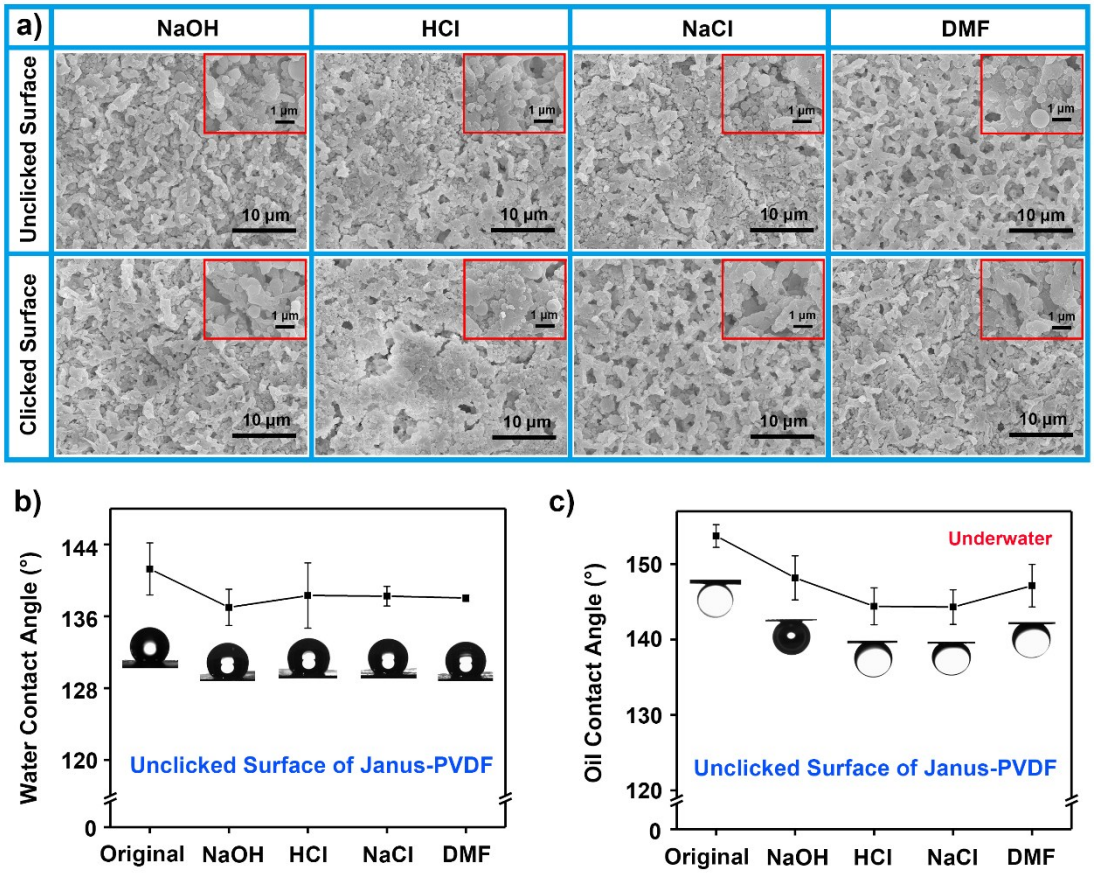

Fig. S13 a) Top SEM images and high-magnification SEM images of the unclicked surfaces and the clicked surfaces of Janus-PVDFs after being kept in aqueous NaOH solution (0.1 M),

aqueous HCl solution (0.1 M), saturated NaCl solution and dimethylformamide (DMF) for 1 h. b) The WCAs of the unclicked surface under after different treatment. c) The UOCAs of the clicked surface under corresponding treatment (the used oil was petroleum ether).

2) The mechanical stability of the Janus-PVDF

The ultrasonic treatment test was also conducted to evaluate the mechanical stability of the Janus-PVDF (Fig. S12). As shown in Fig. S12a, the unclicked surface of the Janus-PVDF remained high-hydrophobic during the whole untrasonic treatment. The slight decrease of WCA after one-hour treatment was due to the partial reduction of silane nanospheres according to the corresponding SEM images (Fig. S12b and S12c). Similar to the Janus-SSM, although the UOCA of the clicked suface of Janus-PVDF gradually dropped with increasing the ultrasonic time, the clicked surface was still underwater high-oleophobic. In addition, the approximate topography of the clicked surface was preserved as exhibited in Fig. S12d. Thus, the as-prepared Janus-PVDF possessed the convincing mechanical stability.

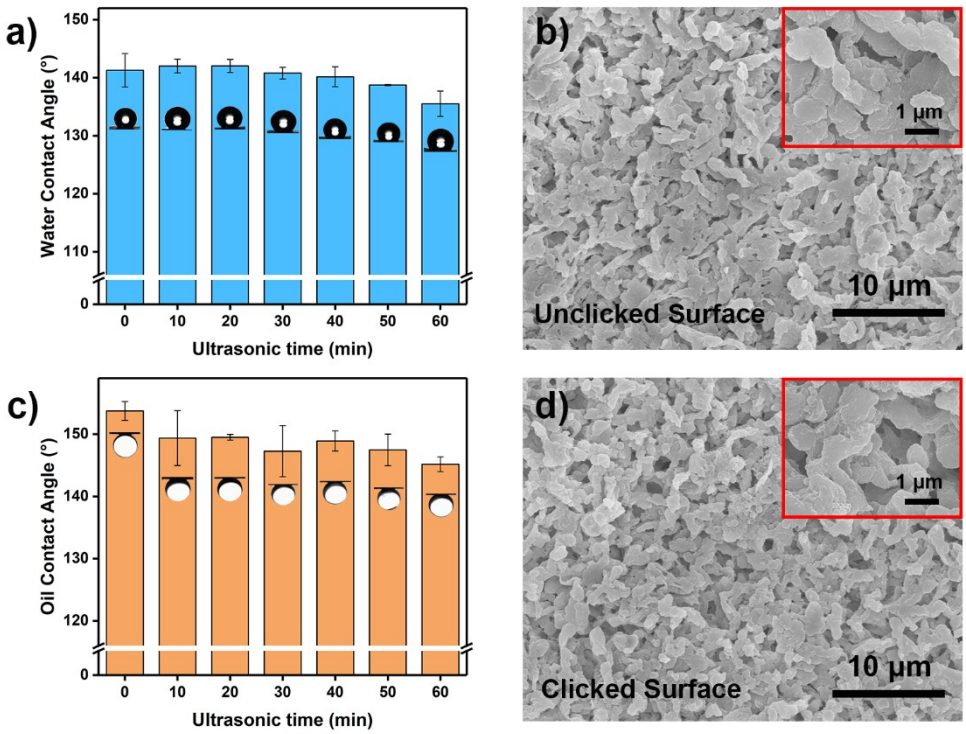

Fig. S14 a) The effect of ultrasonic time on the WCAs of the unclicked surface of the Janus-PVDF. b) Top SEM image and high-magnification SEM image unclicked surface of the Janus-PVDF after ultrasonic treatment in ethanol for 1 h. c) The effect of ultrasonic time on the UOCAs of the clicked surface of the Janus-PVDF. d) Top SEM image and high-magnification SEM image of the clicked surface of the Janus-PVDF after ultrasonic treatment in ethanol for 1 h.

13. Wetting behavior of Janus membranes based on other substrates

As shown in Fig. S8, the proposed method can be applied on other substrates including copper mesh (Cu, with the pore size of 40 μm), nylon membrane (Nylon, with the pore size of 0.8 μm), polypropylene membrane (PP, with the pore size of 0.8 μm) and glass fiber membrane (GF, with the pore size of 0.8 μm). It is worth noting that Janus wettability was exhibited for all four as-prepared substrates, realizing the asymmetric configuration regardless of the material types.

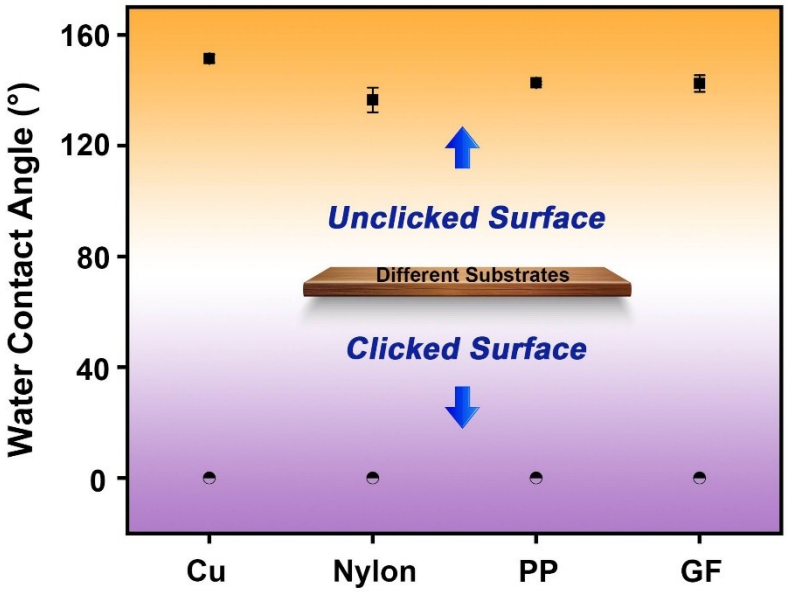

Fig. S15 The water contact angles on the clicked surface and unclicked surface of different Janus membranes based on other substrates.

14. Supplementary Tables S1-S2

Table S1. Comparison of Janus-SSM with other filtration materials for separating immiscible oil/water mixture

Materials	Method	Wettability	Light oil/water mixture	Heavy oil/water mixture	Ref
Hierarchical structured Cu mesh	Electrodeposition	Superhydrophilicity	~ 99.5% (gasoline/water)	/	[1]
Nanofibrous cellulosic membrane	Wet electrospinning	Superhydrophilicity	~ 99.75% (n-hexane/water)	/	[2]
Cu foam with oxy-chloridized nanoparticles	Anodization, etching and calcination	Superhydrophilicity	~ 99% (diesel/water)	/	[3]
SNP/PBZ/PI membrane	Electrospun and dip-coating method	Superhydrophobicity	/	~ 99% (water/dichloromethane)	[4]
HAP nanowires covered paper	Stepwise coating	Superhydrophobicity	/	> 99.2% (water/dichloromethane)	[5]
Janus-SSM	Thiol-ene click reaction	Janus	> 99.99% (n-hexane/water)	> 99.99% (water/ tetrachloromethane)	**This work**

/: Not Provided

Table S2. Comparison of Janus-PVDF with other Janus materials for the emulsion separation

Materials	Method	Wettability contrast	Oil-in-water emulsion	Water-in-oil emulsion	Ref
Janus ZnO-cellulose/MnO_2 membranes	In situ growth technology	153°	99.6% (diesel-in-water)	99.4%(water-in-toluene)	[6]
Janus ceramic membrane	Surface grafting and aeration activated	136°	95.0% (soybean oil-in-water)	99.0%(water-in-hexane)	[7]
Electrospun Janus Membrane	Electrospinning	140°	99.5% (olive oil-in-water)	/	[8]
Janus polymer/carbon nanotube hybrid membrane	Photografting and photopolymerization	133°	/	>99.98%(water-in-toluene)	[9]
Janus CNTs@PAN_{EN} membranes	Electrospinnin and vacuum filtration	140°	~99.7% (petroleum ether-in-water)	~99.2% (water-in-chloroform)	[10]
Janus-PVDF	Thiol-ene click reaction	141°	>99.7% (petroleum ether-in-water)	>99.5% (water-in-petroleum ether)	**This work**

/: Not Provided

15. Supplementary Movies S1-S2

Movie S1. The high-hydrophobic wetting behavior of the unclicked surface.

When the water flows to the surface, the spherical droplets can leave from the surface with low adhesive performance, indicating the high-hydrophobicity of unclicked surface.

Movie S2. The superhydrophilic wetting behavior of the clicked surface.

Water droplets may spread rapidly on the clicked surface, indicating that the superhydrophilicity was endowed on this side on account of thiol-ene click reaction.

16. The detailed discussion of the working patterns of Janus membranes

In general, the working patterns of the reported Janus membranes can be divided into two categories during their applications including the collaborative working pattern and independent working pattern.

1) Collaborative working pattern

In this case, the hydrophobic side and the hydrophilic side work collaboratively to realize the targeted function, which is the type of Janus membranes mentioned in the comment. With regard to this type, most researches mainly focus on the directional liquid transport including water and oil, which can be adjusted by the thickness of hydrophobic side or hydrophilic side. Taking the directional water transport as an example, water drop can penetrate into the membrane from the hydrophobic side to the hydrophilic side when the hydrophobic side is thin enough so that the water drop can contact the hydrophilic side below. Essentially, this transportation behavior depends on the capillary effect which is attribute to Young-Laplace capillary pressures. For the water drop above the membrane, the upward capillary pressure is provided by the hydrophobic side to resist water into the membrane, while the hydrophilic side would produce the downward capillary pressure to attract the water into the membrane. In term of the calculation of the transmembrane pressure which is also investigated in the previous works, the directional transportation is decided by the thickness of hydrophobic side, and the transmembrane pressure can rise significantly with the increased thickness of the hydrophobic layer.

Therefore, the control of the side thickness is of importance for this working pattern (The aforementioned mechanism also applies to the the directional oil transport). Such directional liquid transport makes the oil/water separation possible. Light oil/water mixture is separated with the hydrophobic surface facing up while heavy oil/water mixture is disposed by reversing the membrane orientation, which is different with common superwetting materials. As for the

emulsion separation, the charge on the contact surface and the thickness of hydrophobic side are controlled to realize the demulsification for oil-in-water emulsion in many excellent works. It is worth noting that the collected filtrate is oil phase rather than water and the type of emulsion is restricted. Switchable separation of different kinds of emulsions (oil-in-water and water-in-oil) can also be conducted by this working pattern such as the pressure-responsive carbon nanotube (CNT) Janus membrane reported by the group of Jin. But some challenges still need to be addressed that the applied pressure should be precisely controlled. Thus, the Janus membranes with the collaborative working pattern are mainly used for the disposal of immiscible oil/water mixture or the recovery of valuable oil droplets from oil-in-water emulsions.

2) Independent working pattern

In the other case, the hydrophobic side and hydrophilic side work individually and the overall performance can be promoted. Our Janus materials operate in term of this type of working pattern. In this case, both the hydrophobic side and hydrophilic side are relatively thick, leading to the little effect on each other. The explanation was confirmed by the Low and high-magnification cross-section SEM images of Janus-SSM (Fig. 1d). Lots of different sizes of silane nanospheres were anchored on both sides to form the relatively thick special wettable coating. Janus-SSM can separate light oil/water mixture with the hydrophilic side facing up whereas heavy oil/water mixture can be separated by the hydrophobic side. It can be observed the operating surfaces for oil/water mixtures were opposite to the collaborative working Janus membrane. For emulsion separation, the as-prepared Janus-PVDF as a switchable barrier can realize the controllable oil-in-water and water-in-oil emulsion separation. However, the collaborative working Janus membrane mainly focus on the separation of immiscible oil/water mixtures or single type of emulsions. Our Janus membranes focus on the controllable modes whether immiscible oil/water mixtures or emulsions, achieving the combination of different separation processes through only one membrane.

17. References

[1] E. Zhang, Z. Cheng, T. Lv, Y. Qian and Y. Liu, *J. Mater. Chem. A*, 2015, **3**, 13411-13417.

[2] S. K. Hong, S. Bae, H. Jeon, M. Kim, S. J. Cho and G. Lim, *Nanoscale*, 2018, **10**, 3037-3045.

[3] Z.-Y. Luo, K.-X. Chen, J.-H. Wang, D.-C. Mo and S.-S. Lyu, *J. Mater. Chem. A*, 2016, **4**, 10566-10574.

[4] W. Ma, M. Zhang, Z. Liu, M. Kang, C. Huang and G. Fu, *J. Membr. Sci.*, 2019, **570**, 303-313.

[5] R.-L. Yang, Y.-J. Zhu, F.-F. Chen, D.-D. Qin and Z.-C. Xiong, *ACS Sustainable Chem. Eng.*, 2018, **6**, 10140-10150.

[6] X. Yue, T. Zhang, D. Yang, F. Qiu and Z. Li, *Cellulose*, 2018, **25**, 5951-5965.

[7] D. Ding, H. Mao, X. Chen, M. Qiu and Y. Fan, *J. Membr. Sci.*, 2018, **565**, 303-310.

[8] A. S. Ranganath and A. Baji, *Macromol. Mater. Eng.*, 2018, **303**, 1800272.

[9] J. Gu, X. Peng, C. Jing, J. Zhang, Y. Huang and C. Tao, *ACS Appl. Mater. Interfaces*, 2014, **6**, 16204-16209.

[10] Y. Jiang, J. Hou, J. Xu and B. Shan, *Carbon*, 2017, **115**, 477-485.